# Numerical Study on Supercontinuum Generation in an Active Highly Nonlinear Photonic Crystal Fiber With Anomalous Dispersion

Kyoungyoon Park, Jeongkyun Na, Juhwan Kim, and Yoonchan Jeong, *Member, IEEE*

***Abstract*— We numerically study supercontinuum (SC) generation (SCG) in a rare-earth-doped highly nonlinear photonic crystal fiber (HNL-PCF) with anomalous dispersion (AD) in the sub-picosecond pulse regime. We develop a semi-classical numerical model based on the generalized Ginzburg-Landau equation in order to take account of ultrafast interactions between gain ions and ultra-broadband SC radiation encompassing sub-100-femtosecond solitons. Based on the numerical model, we analyze SCG characteristics of an active HNL-PCF in comparison with a passive-type counterpart, unveiling novel optical gain effects in a highly nonlinear optical fiber with AD. We rigorously investigate gain-induced soliton dynamics, such as soliton-cascade-like behaviors, soliton-quasi-soliton collisions, and phase-matched dispersive wave generation, which eventually contributes to enhancement of energy scaling of SC radiation without incurring considerable degradation of its spectral flatness. We also verify that such superior performance characteristics of an active HNL-PCF make it suitable for the use as a boost amplifier for SC radiation. We think that the findings from this study will incite other subsequent studies on unveiling detailed nonlinear pulse dynamics in various gain-embedded nonlinear optical media.**

***Index Terms*— Optical fiber amplifier, nonlinear optics, supercontinuum generation, ultrashort pulse, anomalous dispersion.**

## I. Introduction

SUPERCONTINUUM generation (SCG) is an extensive spectral broadening process by interplay of linear dispersion and nonlinear optical effects such as self-phase modulation (SPM), four-wave mixing (FWM), Raman scattering, and self-steepening [1]–[3]. In fact, the advent of photonic crystal fibers (PCFs) has remarkably improved the SCG technology thanks to their easy engineering of nonlinearity and group velocity dispersion [4]. The SC radiation generated via a PCF has a wide, flat, and smooth spectrum with high spatial coherence, so that it is widely used in numerous application fields such as microscopy [5], optical sensors [6], optical coherence tomography [7], and biomedicine [8]. While various studies have been conducted on the development of an SC source to improve its bandwidth (BW), coherence, and spectral flatness, etc., their main focus has been, more or less, either on developing a novel-type PCF or on exploiting a novel-type pump source [1], [9], [10]. the development of a novel-type PCF for SCG applications has so far emphasized on engineering its passive characteristics including dispersion and nonlinearity [1]. However, in recent years SCG based on an active-type optical fiber (i.e. a fiber doped with active rare-earth ions) has drawn a significant level of attention for its novel characteristics that cannot be obtained by means of a passive-type PCF, which include its extended power scalability and spectral broadening controllability while maintaining high spectral flatness and temporal coherence [9], [11]–[16]. Taking advantage of both high optical gain and high nonlinearity of such a fiber, an experimental study on SCG using a highly nonlinear erbium-doped optical fiber seeded by 11-ps optical pulses has recently been reported [11]. In this work, high optical gain per unit length ($>10$ dB/m on average) and high spectral broadening per unit length ($\sim$350 nm/m on average) were demonstrated. On the other hand, an extensive numerical study on SCG in an ytterbium (Yb)-doped highly-nonlinear photonic crystal fiber (HNL-PCF) with flattened all-normal dispersion (FAND) seeded by sub-ps ultrafast optical pulses has also been reported [9]. This recent work, as the first theoretical attempt to explain optical gain effects on SCG in the sub-ps ultrafast pulse regime, verified that optical gain can substantially enhance average energy spectral density (AESD) of SC radiation without significantly degrading its spectral flatness and BW. We stress that utilizing an active-type PCF can open up new possibilities for extended power-scaling and controlled spectral broadening of SCG whilst this recent investigation was limited to the case of FAND [9].

On this background, we think that it is necessary to extend the recent investigation on an active HNL-PCF exclusively to the case with anomalous dispersion (AD), because a PCF can be made to operate in either normal or anomalous dispersion regime by simply changing its pitch and hole sizes [17]. However, it is noteworthy that extension of the discussion to the case in the AD regime is not straightforward from the viewpoint of theoretical frameworks: SCG mechanisms in

Manuscript received November 4, 2019; revised February 2, 2020; accepted February 7, 2020. Date of publication February 17, 2020; date of current version February 25, 2020. This work was supported in part by the National Research Foundation of Korea under Grant NRF 2017R1D1A1B03036201 and in part by the Brain Korea 21 Plus Program. *(Corresponding author: Yoonchan Jeong.)*

Kyoungyoon Park, Jeongkyun Na, and Juhwan Kim are with the Department of Electrical and Computer Engineering, Seoul National University, Seoul 06288, South Korea.

Yoonchan Jeong is with the Department of Electrical and Computer Engineering, Seoul National University, Seoul 06288, South Korea, and also with ISRC, IAP, and GSEP, Seoul National University, Seoul 08826, South Korea (e-mail: yoonchan@snu.ac.kr).

Color versions of one or more of the figures in this article are available online at http://ieeexplore.ieee.org.

Digital Object Identifier 10.1109/JQE.2020.2974519

the AD regime are substantially different from those in the FAND regime [3], [9], because SCG in the AD regime tends to trigger sub-ps input pulses to form even shorter pulses, i.e., sub-100-fs solitons as well as dispersive waves (DWs) owing to soliton fission. This aspect contrasts with the case in the FAND regime, in which the input pulse shape is more or less preserved without undergoing any radical changes and evolutions [3], [9]. Thus, if optical gain is involved in SCG in an active HNL-PCF with AD, ultrafast solitons and DWs become to interact with rare-earth ions on very rapid timescales, so that the related SCG dynamics must be treated and analyzed in a drastically different way from the case of SCG in the FAND regime [9]. That is, the rate-equation-based approach utilized in [9] might be no longer appropriate enough for such extremely fast nonlinear interactions in the AD regime. We note that to date only a handful of numerical or theoretical studies have been carried out on analyzing novel characteristic aspects of SCG in active fibers in the AD regime [12], [18]–[20]. In particular, Lei et al. reported that SCG in a Yb-doped fiber (YDF) with AD can be modeled by combining the well-known rate equation and the nonlinear Schrödinger equation (NLSE) when excited by ps pulses [12]. However, it remains questionable to apply the given method to the rigorous analysis of SCG in the sub-100-fs regime, because the interactions between active ions and sub-100-fs ultrafast solitons, which inevitably arise during the SCG process in the AD regime, cannot be modeled properly based on the standard rate equation method. In other words, the standard rate equation method cannot take account of the quantum coherence effects of excited ions, which become non-negligible for the case having timescales within their dipole relaxation time (e.g., $T_2 \sim 16$ fs for Yb ions) [21], [22]. To verify the quantum coherence effects, we analyzed the evolution of a 200-fs soliton pulse in an active fiber with AD by solving the Maxwell-Bloch equations in a direct numerical approach [20]; however, the details of soliton and SCG dynamics in such a condition remained too preliminary. In addition, Arteaga-Sierra et al. reported soliton dynamics in fiber amplifiers, using the complex Ginzburg-Landau equation (CGLE) along with a real-valued super-Gaussian gain spectrum [18]. Although this work focused on the soliton generation in a cascade way and the related pulse dynamics during amplification of low soliton number pulses (i.e. $N < 1$), it did not fully investigate optical gain effects in the context of SCG, the resultant characteristics of which are, in general, quantified by BW, AESD, and spectral flatness, etc. Thus, a comprehensive theoretical study of SCG in an active HNL-PCF with AD in the sub-ps (or sub-100-fs) regime has yet to be carried out to unveil its full details.

Here, in this study we comprehensively and rigorously analyze SCG in an active HNL-PCF with AD seeded by sub-ps optical pulses at a near-zero-dispersion wavelength. In order for properly dealing with sub-100-fs solitons generated by soliton fission during SCG in the AD regime, ultrafast interactions between solitons and active ions are to be described in a semi-classical approach, which is based on the generalized CGLE (GCGLE) derived by combining the NLSE and the Maxwell-Bloch equations (MBEs) in the semi-classical limit [21]–[23]. Based on this theoretical model, we numerically simulate SCG in an active HNL-PCF with AD, and show how the interplay among optical gain, nonlinear effects, and dispersion determines SCG evolution and the related soliton dynamics. Moreover, we numerically demonstrate that an active HNL-PCF with AD can be utilized as a novel external booster amplifier for a soliton-based SC source.


Fig. 1. Conceptual schematic of SCG in an Yb-doped active HNL-PCF. LD: Laser diode, OSA: Optical spectrum analyzer.

## II. Numerical Model

We here consider a conceptual schematic of SCG seeded with sub-ps pulses in an active HNL-PCF as illustrated in Fig. 1. We assume that the active dopants are based on rare-earth ions and the input laser operates in the sub-ps regime with a repetition rate in the MHz range [9]. Because of the short duration of the input pulses, they can evolve in the HNL-PCF under considerable influence of group velocity dispersion and various nonlinear optical effects such as SPM, FWM, Raman scattering, and self-steepening. At the same time, the sub-ps optical pulses propagating in the active HNL-PCF are supposed to be amplified by gain ions during the SCG process. In other words, the input pulses evolve under complex interactions of dispersion, nonlinearity, and optical gain effects.

In general, SCG dynamics involving linear dispersion and various nonlinear effects is described by the NLSE [24], whereas quantum-coherent amplification dynamics in an active medium within very short timescales (e.g., as short as $T_2$ time) is described by the MBEs [20]–[23]. Thus, a self-consistent equation set encompassing the NLSE and the MBEs can surely be a governing master equation set for pulse evolution under effects of dispersion, nonlinearity, and coherent amplification. In fact, the NLSE-MBE equation set is expressed as follows [20]–[23]:

$$\frac{\partial A}{\partial Z} = -\frac{\alpha}{2}A - \sum_{m=2}^{\infty} \frac{i^{m-1}\beta_m}{m!}\frac{\partial^m A}{\partial T^m} + i\gamma_Q N_{tot}\, p + i\gamma\left(1 + \tau_{shock}\frac{\partial}{\partial T}\right) A(Z,T) \int_{-\infty}^{\infty} R(T') \times \left|A(Z, T-T')\right|^2 dT', \quad (1)$$

$$\frac{\partial p}{\partial T} = \left(-\frac{1}{T_2} - i\Delta_a\right) p - \frac{i\mu^2}{\hbar} A n\,, \quad (2)$$

$$\frac{\partial n}{\partial T} = -\frac{1}{T_1^*}\left(n - n_{eq}\right) + \frac{i\left(Ap^* - A^* p\right)}{\hbar}, \quad (3)$$

where $A$, $p$, and $n$ denote the envelope of the optical field, the transition dipole moment, and the normalized population inversion, respectively; $Z$ and $T$ denote the propagation distance

and the time coordinate in the co-moving frame at the envelope group velocity; $\alpha$, $\beta_m$, and $\gamma$ denote the attenuation, the $m$-th order dispersion, and the nonlinear coefficients; $\tau_{shock}$ denotes the shock coefficient for self-steepening, which is usually characterized by the inverse of the center angular frequency (i.e., $1/\omega_0$). The nonlinear response function is expressed by $R(T) = (1-f_R)\delta(T) + f_R h_R(T)$, which includes SPM and Raman response, where $f_R$ is usually given by 0.2 for typical silica fibers (see [9] for details of the Raman response function). As for the dopant parameters, $\gamma_Q$ denotes the polarization coupling constant, $N_{tot}$ the number density of dopants, $T_2$ the dipole relaxation time, $\Delta_a$ the frequency offset of the center frequency of the optical pulses from the amplification frequency $\omega_a$, and $\mu$ the transition dipole moment. $T_1^*$ and $n_{eq}$ denote the effective spontaneous decay time (or the effective pumping time) and the population inversion at equilibrium, which are dependent on pumping rate $R_p$ and the spontaneous decay time $T_1$. It is noteworthy that Eqs. (2) and (3) are derived, under an assumption that Yb ions have a four-level energy structure: $T_1^*$ and $n_{eq}$ are thus expressed as $T_1^* = T_1/(R_p T_1 + 1)$ and $n_{eq} = R_p T_1/(R_p T_1 + 1)$ [25].

However, without loss of generality it is known that in the case of a fiber-optic gain medium of rare-earth ions, the Bloch vector does not change much in the vertical direction even when considering coherent interactions between optical fields and gain ions [26]. This applies to our case, because the soliton energy level of interest, which is typically in a pico-joule order, is much smaller than the saturation energy of gain ions, which is typically in a micro-joule order. Consequently, the amount of the normalized population inversion change during coherent amplification becomes nearly negligible [23], [26]. In fact, it has been reported that its typical change is quantified as small as below $10^{-5}$ in room-temperature conditions [23]. Thus, in this limit we readily derive the GCGLE from the NLSE-MBE set as follows (see [26] for details of the derivation):

$$\frac{\partial A}{\partial Z} = -\frac{\alpha}{2}A - \sum_{m=2}^{\infty}\frac{i^{m-1}\beta_m}{m!}\frac{\partial^m A}{\partial T^m} + i\gamma\left(1+\tau_{shock}\frac{\partial}{\partial T}\right) \times A(Z,T)\int_{-\infty}^{\infty} R(T')\left|A(Z,T-T')\right|^2 dT' + \frac{1}{2\pi}\frac{g}{2}\int_{-\infty}^{\infty}\frac{\tilde{A}(Z,\omega-\omega_0)}{1-i(\omega-\omega_a)T_2}e^{-i(\omega-\omega_0)T}d\omega\,. \quad (4)$$

In Eq. (4), the saturated gain coefficient $g$ is given by $g = g_{us}/\left(1 + N^* E_{pulse}^{eff}/E_{sat}\right)$, where $N^*$ is the number of pulses that pass through gain ions over the time $T_1^*$ with a repetition rate of $1/T_R$, and $g_{us}$ is the unsaturated gain coefficient expressed as $\sigma_s N_{tot} n_{eq}$. We note that both $T_1^*$ and $g_{us}$ depend on the pumping rate. During the derivation of Eq. (4), the effectively absorbed pulse-energy $E_{pulse}^{eff}$ is obtained as [26]:

$$E_{pulse}^{eff} = \frac{1}{2\pi}\int_{-\infty}^{\infty}\frac{\left|\tilde{A}(Z,\omega-\omega_0)\right|^2}{1+(\omega-\omega_a)^2 T_2^2}d\omega. \quad (5)$$

It is noteworthy that transient responses of gain ions for ultrafast pulses described in Eq. (2) are sufficiently taken into account in the derivation of Eqs. (4) and (5), which are, however, completely ignored in the rate-equation-based approximation [27]. We stress that Eq. (5) indeed exhibits an important aspect of the ultrafast interactions between broadband SC radiation and gain ions: It tells how the effectively absorbed pulse energy is estimated when the spectral BW of the input pulses is significantly larger than that of gain ions: The contributions of the spectral components of the input pulses outside the gain BW are taken into account via the weighting function as given in the denominator of Eq. (5). This plays a critical role in properly describing the gain saturation effect by the repetitive ultrafast SC pulses [26]. Otherwise, the coherent absorption of the input SC pulses by gain ions might considerably be overestimated [26].

We now investigate SCG in an HNL-PCF having AD. It is launched by input pulses centered at 1064 nm having a hyperbolic secant profile such as $A(T) = P_0^{1/2}\mathrm{sech}(T/T_0)$ with a 176-fs pulse duration (full width at half maximum: FWHM) and a 0.6-nJ pulse energy, which correspond to a 3.0-kW peak power and a soliton number $N$ of 9. It is noted that the soliton number $N$ is defined as $(L_D/L_{NL})^{1/2}$, where $L_D$ and $L_{NL}$ denote the dispersion and nonlinear lengths, respectively [1], [24]. The high soliton numbers mean that we are dealing with the case where $L_D$ is much longer than $L_{NL}$. We assume the passive parameters of the HNL-PCF as follows: The fiber length $L$ is in the range of around 1 m. The fiber dispersion coefficients at 1064 nm are given by $\beta_2 = -11.2$ ps$^2$/km, $\beta_3 = 8.0\times10^{-2}$ ps$^3$/km, $\beta_4 = 9.9\times10^{-5}$ ps$^4$/km, $\beta_5 = 1.2\times10^{-7}$ ps$^5$/km, and $\beta_6 = 4.0\times10^{-11}$ ps$^6$/km, which result in AD with a negative slope at around 1064 nm and the zero-dispersion wavelength (ZDW) at 975 nm [15]. The fiber attenuation is low enough to be ignored, taking account of the short fiber length. The fiber nonlinear coefficient $\gamma$ is given by 29 W$^{-1}$km$^{-1}$. On the other hand, we assume the active parameters of the HNL-PCF as follows: When operating in non-zero gain, the fiber gain is based on excited Yb ions, matched for the amplification of the input pulses centered at 1064 nm. The spontaneous decay time $T_1$ and the dipole relaxation time $T_2$ of the Yb ions are given by 0.8 ms and 16 fs, respectively. The latter yields the Yb ions' gain BW of 20 THz. The unsaturated gain coefficient $g_{us}$ of the active HNL-PCF is set to 40 dB/m, thereby being capable of resulting in the overall energy gain at the fiber end of $\sim$10 dB along with the other given parameters. We note that the unsaturated gain coefficient corresponds to a core absorption rate of 178 dB/m at 976 nm, which is readily achievable with current fiber fabrication techniques [28]. The effective saturation energy per single-pulse denoted as $E_{sat}/N^*$ is set to 3 nJ, which is a typical value for a Yb-doped fiber amplifier with a MHz-level repetition rate [9]. We summarize all the parameters in Table 1, which will remain unchanged unless stated otherwise. Finally, we solve Eqs. (4) and (5) by utilizing the 4-th-order Runge-Kutta method in the Fourier domain [29], for which we determine the number of grids and the time window size to be $2^{15}$ and 90 ps, respectively, allowing for

TABLE I
SIMULATION PARAMETERS

| Parameter | Value | Parameter | Value |
|---|---|---|---|
| $\beta_2$ [ps$^2$/km] | −11.2 | $g_{us}$ [dB/m] | 0 ~ 40 |
| $\beta_3$ [ps$^3$/km] | $8.0\times10^{-2}$ | $T_1$ [ms] | 0.8 |
| $\beta_4$ [ps$^4$/km] | $9.9\times10^{-5}$ | $T_2$ [fs] | 16 |
| $\beta_5$ [ps$^5$/km] | $1.2\times10^{-7}$ | $E_{sat}/N^*$ [nJ] | 3 |
| $\beta_6$ [ps$^6$/km] | $4.0\times10^{-11}$ | $P_0$ [kW] | 1 ~ 10 |
| $\gamma$ [W$^{-1}$km$^{-1}$] | 29 | $T_0$ [fs] | 100 |
| $L$ [m] | 0.74 ~ 1.60 | | |

both SC radiation's temporal and spectral spreads to fit into the time and frequency windows of 360 THz. We calculate the spectral flatness measure (SFM) of the calculated SC radiation utilizing the formula specified in [10].

## III. NUMERICAL RESULTS AND DISCUSSION

### A. Gain Effects on SCG in the AD Regime

We first investigate the gain effects on SCG in the HNL-PCF with AD specified in the preceding section, comparing two distinct cases: One is the case when the HNL-PCF works as a passive (undoped) fiber, i.e., $g_{us} = 0$ dB/m, as similar as the passive PCFs with AD reported in the literature [1]–[3], [30]. The other is the case when it works as an active fiber with $g_{us} = 40$ dB/m. We note that all the fiber parameters except the gain coefficient are the same for both cases as specified in the preceding section, and that the fiber length is set identically to 1.6 m for both cases. We numerically analyze both cases based on Eqs. (4) and (5), and plot the temporal and spectral evolutions of the corresponding SC radiation in Figs. 2(a)-2(d). We also calculate 20-dB BWs and AESDs of them with respect to propagation distance in Figs. 2(e) and 2(f). We note that the AESD is given by the mean energy spectral density within 20-dB BW of the given SC radiation. When the HNL-PCF works as a passive fiber as shown in Fig. 2(c), one can see that the input pulse ($N = 9$) undergoes the typical soliton fission process such that the input pulse splits into multiple fundamental solitons, generating DWs. The DWs are phase-matched with the corresponding fundamental solitons. These DWs are commonly known as non-solitonic radiation (NSR) or Cherenkov radiation [2]. The emitted solitons undergo deceleration, being red-shifted by Raman scattering. Time delays of these solitons continually increase, eventually giving rise to collisions with the DWs in the normal dispersion (ND) region. The DWs are then trapped by the decelerating Raman solitons, being blue-shifted under the phase and group-velocity matching conditions with the corresponding Raman solitons [2], [30]. Consequently, the resultant SC spectrum is extensively broadened by the Raman solitons and DWs as shown in Fig. 2(a). However, we note that as the solitons are consecutively released from the input pulse, its effective soliton number gradually decreases. Thus, once the effective soliton number has become less than unity, the soliton fission process is eventually terminated [1]. In contrast, when the optical gain is turned on, the dynamics associated with soliton fission becomes substantially different from that of the passive case: The 'pulse remnant' [18], which

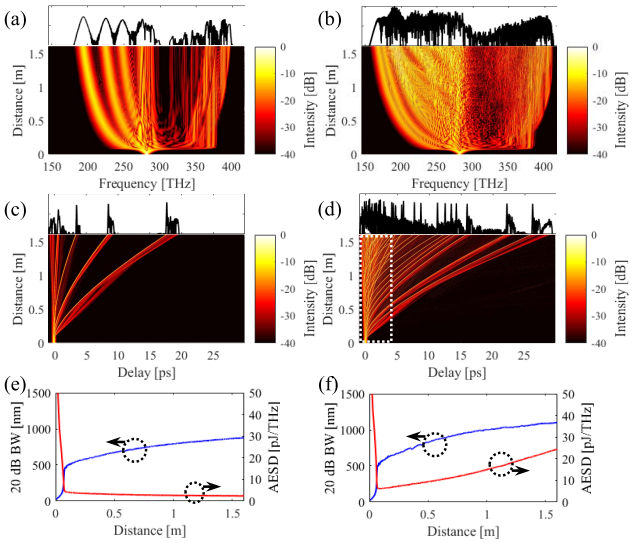


Fig. 2. Evolutions of SC radiation in passive and active HNL-PCFs. (a) and (b): Spectral evolutions in the passive HNL-PCF ($g_{us} = 0$ dB/m) and in the active HNL-PCF ($g_{us} = 40$ dB/m), respectively. (c) and (d): Temporal evolutions in the passive case and in the active case, respectively. (e) and (f): Evolutions of 20-dB BW and AESD in the passive case and in the active case, respectively. Note that the output spectra and temporal traces are put on top of the figures of (a)-(d), respectively.

is the part of the input pulse remaining after the soliton fission or breakup at $z = 0.07$ m, continues to emit fundamental solitons as shown in Fig. 2(d). This is due to the fact that it can continually gain extra energy via the amplification process by excited gain ions, being able to be recovered from the energy loss by emitting solitons. As a result, the recovered pulse remnant can keep emitting fundamental solitons more frequently and extensively, being red-shifted and spreading widely over the AD frequency region by Raman scattering in the fiber. In addition, the DWs generated under the phase and group-velocity matching conditions with the solitons are also widely distributed over the ND frequency region. In fact, the high nonlinearity combined with the high gain makes the SC radiation more densely distributed in both time and frequency domains.

The impacts of gain effects on the SC radiation are clearly visible in the BW and AESD as shown in Figs. 2(e) and 2(f). In the passive HNL-PCF case, the BW increases rapidly as the input pulse reaches the soliton-fission length, and then keeps increasing slowly owing to the Raman red-shifts of the emitted solitons and the blue-shifts of the trapped DWs after the fission length. In this passive case the total energy of the SC radiation obviously remains constant, so that the increase in the BW implies the decrease of the AESD. That is, the AESD rapidly decreases until the fission length, and then keeps decreasing slowly. In contrast, when the optical gain is involved in, the total energy of the SC radiation is no longer constant, thereby being able to increase even during the SCG process. However, we note that the BW does not increase substantially in comparison with the passive case. This is due to the fact that the fission length is as short as ~0.2 m in the given conditions, so that the soliton number of the input pulse cannot grow substantially in such a short distance.

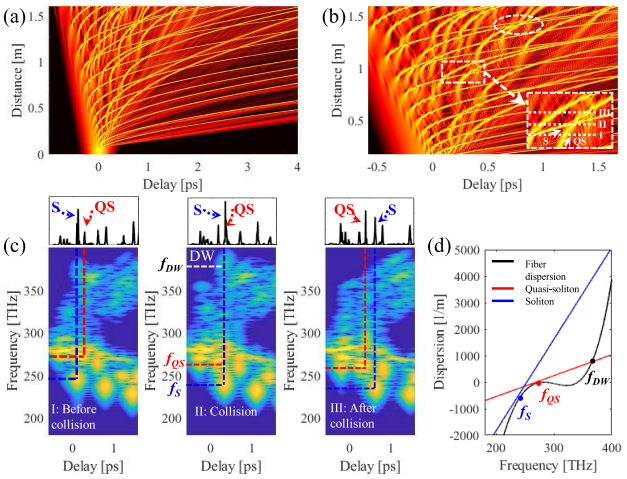


Fig. 3. Detailed soliton formation and dynamics in the active HNL-PCF. (a) Zoomed-in image of the part enclosed by the rectangle in a white-dashed line in Fig. 2(d). (b) Formation of solitons and QSs, and their collision dynamics. The inset is the zoomed-in image of the part enclosed by the rectangle in a white-solid line in (b). (c) Spectrograms and the linear-scale intensity profiles corresponding to Stage I, Stage II, and Stage III. S: Soliton; QS: Quasi-soliton. (d) Dispersion relations of the corresponding soliton, QS, and the HNL-PCF.

In other words, the frequency red-shift of the first emitted soliton, which crucially determines the BW of the generated SC radiation, is not substantially larger than that in the passive case, even though it is surely larger than that in the passive case. As a result, the extra energy supplied into the SC radiation via the amplification process through excited gain ions leads to a substantial amount of increase in the AESD. Whilst the AESD initially decreases until the fission length, it continues to increase afterwards as shown in Fig. 2(f). This aspect is in stark contrast to the passive case, in which the AESD monotonically decreases through the whole fiber length.

The detailed soliton formation and dynamics in the active HNL-PCF case are further illustrated in Fig. 3(a) and 3(b), which are, in fact, the zoomed-in images of the part enclosed by the rectangle in a white-dashed line in Fig. 2(d). In Fig. 3(a), we note that the input pulse breaks up into multiple fundamental solitons, also generating DWs after the soliton fission length. Actually, the pulse remnant is continually amplified by excited gain ions, so that it consecutively emits fundamental solitons every time it has gained sufficient energy to do so by amplification. The fundamental solitons characteristically undergo red-shifts and group delays by Raman scattering. In fact, these features are very similar to those observed in the 'soliton cascades' reported in [18], where the dynamics of soliton cascades was numerically studied particularly for the case of the amplification of ultrashort optical pulses having energy less than required to form a soliton of an equal pulse width in an active fiber with moderate gain and moderate nonlinearity parameters. Contrasting to the soliton cascades previously reported [18], we stress that the active HNL-PCF in this current investigation has substantially high gain and high nonlinearity parameters, and that the input pulse also has a substantially high soliton number. Consequently, solitons are generated not only from the leading part of the pulse remnant but also from the trailing part of it, as shown in Fig. 3(a). Formation of such solitons is further zoomed in Fig. 3(b): In particular, we note that a new type of pulse starts to form in the region enclosed by the rectangle and ellipse in a white-dashed line in Fig. 3(b). Although the pulse is in an intermediate stage before being able to form an ordinary soliton shape from the viewpoint of its spectrogram features shown in Fig. 3(c), we may well call it a 'quasi-soliton (QS)' because it approximately exhibits characteristic features of a soliton, eventually evolving into an ordinary one afterwards, which include continual red-shift and distinct localization in the spectro-temporal domain [31]. These QSs tend to undergo specific group delays by Raman scattering in the given situations, thereby resulting in collisions with nearby ordinary solitons or other QSs, while travelling at different group velocities as illustrated in Fig. 3(b). Actually, we have analyzed the collision process incurred by one of the QSs in more detail by means of the spectrogram analysis into three different stages of I, II and III [see the inset of the Fig. 3(b)], and show their temporal and spectral evolutions in Fig. 3(c) [1].

In Stage I, which is the period before the collision occurs, the soliton at ~250 THz (at a low frequency) is initially preceding the QS at ~270 THz (at an intermediate frequency). The soliton's peak power is higher than that the QS's. By the way, the soliton's group delay rate is also higher than the QS's owing to the fact that both are in the AD regime.

Thus, they are gradually coming closer in this stage. In addition, in this stage the trace of the QS represented in the spectrogram has not been localized as clearly as that of the soliton. In Stage II, it is very intriguing to note that a high-frequency DW at ~370 THz is generated while the soliton and the QS collide. We cannot explain the frequency of this DW in terms of FWM involving the corresponding soliton and QS. We instead attribute its generation to the consequence of the energy shed from the QS during its transition towards an ordinary soliton after the soliton-QS collision: We have numerically verified it, analyzing the dispersion relations of the corresponding soliton, QS, and the HNL-PCF, as shown in Fig. 3(d). We note that the dispersion relation line for the QS intersects that of the HNL-PC approximately at the center frequencies of the QS and the DW given in the Fig. 3(c), which are also denoted with the solid circles in red ($f_{QS} = 268$ THz) and in black ($f_{DW} = 366$ THz) in Fig. 3(d), respectively. This implies that the DW is indeed likely to be phase-matched with the QS in the HNL-PCF [2], [24].

On the other hand, the dispersion relation line of the soliton seems to intersect that of the HNL-PCF at the even higher frequency ($f_S = 410$ THz) if we find one for a phase-matched DW. However, it is hard to expect such a case to occur by means of the soliton itself, because it has already been formed as an ordinary soliton even earlier than this stage, thereby only being able to give rise to a very limited energy shed by the soliton-QS collision unless the collision is extremely strong [2], [21]. We confirm that there are no additionally significant spectro-temporal components beyond the range shown in Fig. 3(c). That is, the phase-matched DW generation by the soliton itself has already occurred while the soliton was initially formed from the input pulse at the even earlier stage, in which the frequency of the soliton was

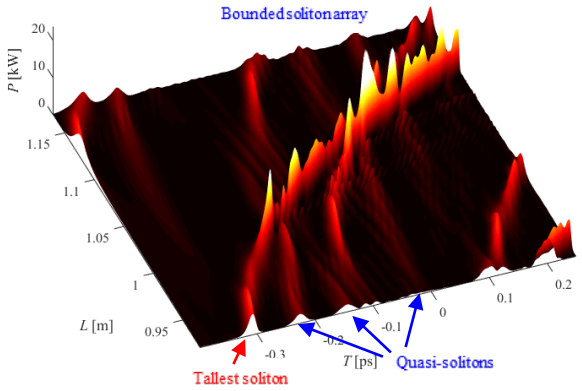


Fig. 4. Detailed three-dimensional view of the NC dynamics in the active HNL-PCF observed from Fig. 3(b).

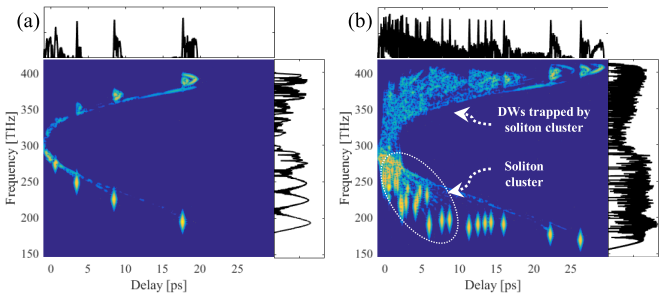


Fig. 5. Output spectrograms for the passive and active HNL-PCFs. (a) Passive HNL-PCF case ($g_{us} = 0$ dB/m). (b) Active HNL-PCF case ($g_{us} = 40$ dB/m).

even higher because it had not undergone the corresponding red-shifts by Raman scattering. Anyhow, after the soliton-QS collision, the spectrogram trace of the QS gradually becomes further distinctive in the spectro-temporal domain and eventually turns into that of an ordinary soliton in State III as shown in Fig. 3(c). We emphasize that generation of these high frequency DWs via soliton-QS collisions is one of the characteristic features of SCG in an active HNL-PCF with high gain and high nonlinearity. Another astonishing aspect of the soliton dynamics in this active HNL-PCF is that a bunch of solitons and QSs can collide together at the same time: See the extreme event at $z = \sim$1.4 m enclosed by an ellipse in a white-dashed line in Fig. 3(b). We suspect that this happens because DWs trapped by the soliton pair along with the QSs are reflected back and forth among them, subsequently pulling them closer to each other [32]. In such an eventful circumstance, one may be able to observe a variety of extreme events, such as optical Newton's cradle (NC) dynamics [31], optical rogue wave generation [18], [32]–[35], and optical event horizon [36]. In fact, in an active HNL-PCF, where a large set of solitons are are generated owing to optical gain, NC dynamics may occur. That is, the high energy of the first soliton of the bounded soliton array is transferred to the last soliton by a series of soliton collisions. As shown Fig. 4 that is taken from Fig. 3(b), a non-uniform soliton chain is formed by soliton fission, modulation instability, and optical gain at $z\sim$0.9 m. The NC dynamics, which causes continual collisions within the non-uniform soliton chain, indicates that the last soliton of the chain takes significantly high peak power, thereby escaping out of the bounded soliton array at $z\sim$1.1 m. This aspect is quite similar to the NC dynamics observed in a passive fiber presented in [31], where non-uniform soliton chains are generated by the third-order dispersion (TOD) of the fiber. However, in an active HNL-PCF, they are generated not only by the TOD, but also by the amplification of the pulse remnant via optical gain. This makes clear contrast to the passive fiber case. In addition, other extreme events such as optical rogue wave generation and optical event horizon are beyond the scope of this study and should be dealt with in further detail elsewhere.

We can see additional impacts of gain effects on the SC radiation when we compare side by side the resultant spectrograms with and without optical gain: Fig. 5(a) represents the spectrogram with the output snap shots for the temporal intensity and spectral power density profiles in the passive HNL-PCF case, in which only four solitons are generated at AD frequencies along with the corresponding DWs at ND frequencies trapped by the solitons. In contrast, Fig. 5(b) represents the spectrogram with the output snap shots for the temporal intensity and spectral power density profiles in the active HNL-PCF case, in which a huge number of solitons and DWs are generated at the same time, forming a soliton cluster densely packed in the range of 0 to $\sim$10 ps and the corresponding "sea of DWs". This feature again signifies that the DWs trapped by the soliton cluster along with QSs collide back and forth with the number of solitons and QSs in the cluster, provoking extreme events such that they cover up the temporal and spectral spaces otherwise could have remained nearly empty as in the passive case. This eventually results in a substantial level of improvement in terms of SFM for the output SC radiation as can be noticed in Fig. 5: We have calculated the SFM values in 20-dB BW for both passive and active cases, which are given by 0.19 and 0.26, respectively.

### *B. Comparative Analysis of Energy-Scaling Schemes for SCG*

In the preceding section, we have verified the novel characteristic features of SCG in an active HNL-PCF with AD in terms of AESD and SFM. However, one may think that scaling of AESD of SC radiation is still possible with a passive HNL-PCF if the input pulse energy is scaled up in advance to the passive HNL-PCF. This can be realized by simply inserting a lumped amplifier between the seed source and the passive HNL-PCF as the cases demonstrated in most SCG experiments [13], [37], [38]. (Alternatively, one one may think of direct amplification of the SC radiation obtained after the passive HNL-PCF; however, this cannot be an effective way, because there is no practical amplifier whose gain BW can cope with the huge BW of the SC radiation extending to several hundreds of nanometers [39]. Notwithstanding, we will also investigate this specific situation in the next section.) In this configuration, unlike the active HNL-PCF case, the amplification and SCG processes are separate, thereby taking place one by one. We thus investigate this passive HNL-PCF case with initially energy-boosted input, and compare its characteristics with those of the active HNL-PCF case. For the sake of a fair

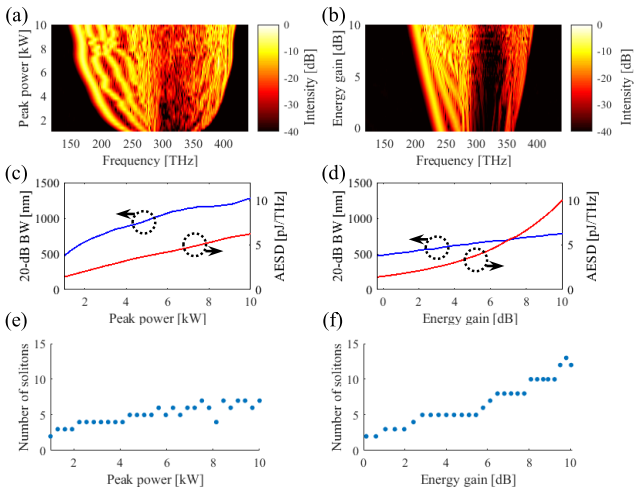


Fig. 6. Characteristics of the passive HNL-PCF case combined with initially energy-boosted input and the active HNL-PCF case. (a) and (b): Spectral evolutions in the passive HNL-PCF case with initially energy-boosted input and in the active HNL-PCF case, respectively. (c) and (d): Evolutions of 20-dB BW (blue) and AESD (red) in the passive HNL-PCF case with initially energy-boosted input and in the active HNL-PCF case. (e) and (f): Total numbers of solitons generated in the passive HNL-PCF case with initially energy-boosted input and in the active HNL-PCF case, respectively. It is noted that the figure set on the left side, i.e., Figs. 6(a, c, e) is for the passive HNL-PCF case with initially energy-boosted input, and that the figure set on the right side, i.e., Figs. 6(b, d, f) is for the active HNL-PCF case.

comparison, we assume that the total energy scaling factors are identically set from 1 to 10 dB in 1 m of fiber length for both cases. In other words, for the former case, we vary the peak power of the input pulse from 1 to 10 kW, which corresponds to the total energy of the input pulse from 0.2 to 2 nJ. For the latter case, we vary the unsaturated gain coefficient from 0 to 33.4 dB/m with the peak power of the input pulse fixed at 1 kW, which results in exactly the same amounts of the total energy or the total energy scaling factor of the resultant SC radiation as the former case. We note that we keep all other pulse and fiber parameters the same as those used in the preceding section for both cases. We present the corresponding numerical simulation results in Fig. 6. As shown in Fig. 6, even though the total energy of the output SC radiation is the same for both cases, their specific characteristics in terms of BW, AESD, and the number of solitons generated are drastically different. In the former case, as the input peak power increases, the BW of the SC radiation grows considerably as shown in Figs. 6(a) and 6(c). This is due to the fact that in the case of SCG pumped at an AD frequency, the BW of the SC radiation is, in principle, determined by how far the first-ejected soliton shifts by Raman scattering [1], which is in turn proportional to the peak power of the input pulse [40]. In contrast, in the latter case, the BW of the SC radiation does not grow as considerably as in the former case. The reason for this consequence is that the peak power of the input pulse cannot grow as immediately as the amplification process by excited gain ions until reaching the fission length as already verified in Fig. 2(f). For example, if we suppose that the total energy of the SC radiation is scaled up by 10 dB for both cases, the former case results in an immediate 10-dB increase in the peak power of the input pulse whereas in the latter case the total 10-dB energy gain is distributed in the whole SC radiation throughout the whole length of the fiber. Consequently, the peak power of the first-ejected soliton in the latter case cannot be as high as that in the former case.

Thus, without loss of generality, the BW growth of the latter case becomes insignificant relative to the former case. Since the total energy of the output SC radiation is assumed to be the same in both cases, the narrower BW implies the higher AESD. Therefore, the AESD through the active HNL-PCF should be by far higher than that through the passive HNL-PCF as shown in Figs. 6(c) and 6(d). We highlight that the high energy injected into the passive HNL-PCF by means of the input pulse is used to broaden the BW of the SC radiation, whereas the high energy injected by means of excited gain ions progressively amplifies the SC radiation throughout the whole fiber length, thereby being able to increase the AESD more effectively. The difference of these characteristic features can also be manifested by the number of solitons generated in both cases as shown in Figs. 6(e) and 6(f). We note that substantially more solitons are generated in the active case than in the passive case. [In Figs. 6(e) and 6(f), the slight fluctuations of the soliton numbers are due to the fact that the solitons that coincidently collide at the fiber end are counted as one pulse.] In result, we stress that an active HNL-PCF has a clear advantage over its passive counterpart in terms of AESD scaling.

### *C. Direct Amplification of SC Radiation*

In the preceding two sections, we have discussed that the distinct characteristic features of SCG via an active HNL-PCF in comparison with its passive counterparts. In this section, making the most of the advantageous features of SCG via an active HNL-PCF, we propose and verify that an active HNL-PCF can also be exploited for amplifying broadband SC radiation that has already been produced via other passive-type PCFs. Perhaps, one may think of the use of a conventional amplifier based on a low-nonlinearity YDF to amplify such SC radiation. However, we should note that the gain BW of Yb ions is limited just to ~20 THz, which is far too narrow to amplify the whole SC radiation whose BW can typically go beyond 200 THz. In fact, there are no other practical candidates to deal with such broadband radiation. Thus, it is necessary to exploit the characteristic features of an active HNN-PCF since we have already verified in the preceding section that the high nonlinearity combined with high gain via an active HNL-PCF can extend the gain effects to an even wider spectral range than the nominal gain BW that rare-earth ions can provide. In this regard, we further investigate the functionality of an active HNL-PCF as an external amplifier capable of amplifying broadband SC radiation, in comparison with a conventional amplifier based on a low-nonlinearity YDF. For the sake of a fair comparison, we assume that SC radiation inputs for both cases are identically generated by the passive HNL-PCF investigated in Section 3.1, the characteristics of which are the same as those already shown in Figs. 2(a) and 2(c). That is, they identically have a total energy of ~0.6 nJ and a 20-dB BW of 792 nm. The nonlinear

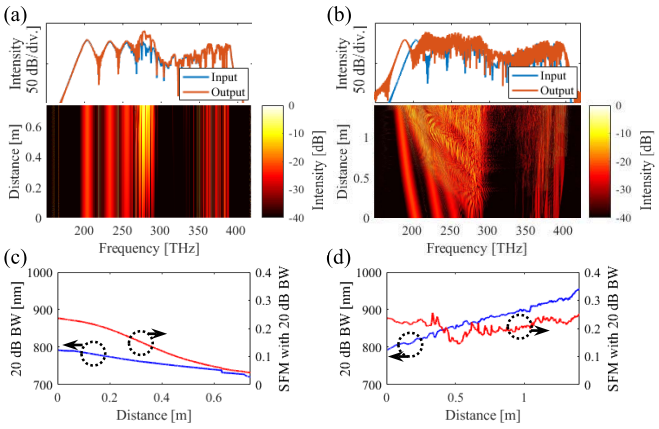


Fig. 7. Characteristics of the passive HNL-PCF case combined with a conventional amplifier based on a low-nonlinearity YDF and the active HNL-PCF case. (a) and (b): Spectral evolutions in the passive HNL-PCF case combined with a conventional amplifier based on a low-nonlinearity YDF and in the active HNL-PCF, respectively. (c) and (d): Evolutions of 20-dB BW (blue) and SFM (red) within the 20-dB BW in the passive HNL-PCF case combined with a conventional amplifier based on a low-nonlinearity YDF and in the active HNL-PCF, respectively.

coefficient of the YDF is set to a typical value of silica-based fibers (i.e., $\gamma = 1$ W$^{-1}$km$^{-1}$). The length of each fiber is determined to yield 10-dB energy gain for each case for a fair comparison, so that the YDF and the active HNL-PCF lengths are given by 0.74 and 1.40 m, respectively. All other fiber parameters remain the same as in the preceding sections.

The spectral evolution and the output spectrum of the SC radiation amplified by the YDF are shown in Fig. 7(a), which indicates that the amplified SC radiation considerably loses its initial BW because only a fraction of the SC radiation that lies within the gain BW of Yb ions (∼20 THz) is amplified. This consequence in turn gives rise to substantial degradation in SFM as shown in Fig. 7(c). The SFM values within 20-dB BW for the SC radiation before and after amplification are calculated to be 0.24 and 0.04, respectively. In contrast, the output SC radiation amplified by the active HNL-PCF yields very promising outcomes in terms of BW and SFM as shown in Fig. 7(d): The BW further increases by a small amount owing to the extra red-shift of the first-emitted soliton by Raman scattering, and it still produces a flat SC radiation, maintaining nearly the same SFM as the original value. The SFM values in 20-dB BW before and after amplification are calculated to be 0.24 and 0.25, respectively. These characteristics are superior to those with the conventional YDF case. In this light, an active HNL-PCF with AD should be a good candidate for an external amplifier for soliton-based SC radiation since it can scale up the power of SC radiation without incurring degradation of SFM as in the case of an active HNL-PCF with FAND for amplifying coherent SC radiation [9].

## IV. Conclusion

We have numerically analyzed SCG in an active HNL-PCF with AD having a negative slope excited by sub-ps ultrafast input pulses, based on the GCGLE derived from the NLSE-MBE model capable of dealing with ultrafast solitons' nonlinear interactions with gain ions within their dipole relaxation time.

We have first investigated optical gain effects on the SCG process, analyzing spectro-temporal characteristics of the HNL-PCF for two distinct cases with and without optical gain, and verified that distributed amplification of SC radiation via excited gain ions substantially improves the AESD without incurring degradation of the SFM of the corresponding SC spectrum. We have also figured out that during the SCG process, a multitude of solitons and QSs with different group velocities are generated and intricately collide, and these collisions also produce high-frequency DWs particularly phase-matched with QSs. We note that in the case of the active HNL-PCF, amplification of the pulse remnant is possible even after soliton fission, because distributed gain ions continually supply energy to SC radiation, which in turn leads to generation of a multitude of additional solitons (i.e., a soliton cluster). In fact, the high nonlinearity combined with high gain creates the soliton cluster and the corresponding high-frequency DWs, so that the energy spectra of them are more densely and evenly distributed across the wide BW of SC radiation than in the case of the passive HNL-PCF. We have also verified that the active HNL-PCF as an all-in-one structure capable of combining high nonlinearity and high gain exhibits much superior performance to the passive HNL-PCF from the viewpoint of AESD and SFM of the resultant SC radiation, even when an auxiliary lumped fiber amplifier is inserted before or after the passive HNL-PCF. In other words, the continual amplification of SC radiation distributed along the highly nonlinear fiber offers a great advantage in power-scaling of SC radiation, firmly keeping good AESD and SFM characteristics.

In addition, we would like to compare the characteristic features of the HNL-PCF with AD with those of the HNL-PCF with FAND previously studied [9]. The common feature of them is that when high nonlinearity is combined with high gain distributed in the fiber, optical gain effects lead to substantially improved AESD without incurring significant degradation of SFM, regardless of their dispersion properties. However, the individual physical mechanisms and dynamics behind the results are largely different. Whilst in the case of the HNL-PCF with FAND the energy spectrum of the SC radiation is extended by coherent processes, such as SPM and optical wave breaking, in the case of the HNL-PCF with AD it is obtained by incoherent processes, such as modulation instability, soliton fission, and Raman scattering. Another distinct feature between them is that whilst the overall BW of the resultant SC radiation does not expand with the distributed gain effects in the case of HNL-PCF with FAND when it is used as a boost amplifier for the SC radiation, it does expand a bit in the case of the HNL-PCF with AD. This is due to the fact that in the latter case, the first ejected soliton undergoes a considerable amount of amplification by the distributed gain effects whereas in the former case the SC radiation tends to preserve its original temporal shape throughout the whole fiber length [9].

We believe that our numerical study on SCG in an active HNL-PCF with AD will pave the way to advances in novel SCG technology in the sub-ps regime, and also hope that this

study will be helpful for other subsequent ones on unveiling detailed nonlinear pulse dynamics in various optical gain-embedded nonlinear media.

## REFERENCES


[1] J. M. Dudley, G. Genty, and S. Coen, "Supercontinuum generation in photonic crystal fiber," *Rev. Mod. Phys.*, vol. 78, p. 1135, Oct. 2006.

[2] D. V. Skryabin and A. V. Gorbach, "Colloquium: Looking at a soliton through the prism of optical supercontinuum," *Rev. Mod. Phys.*, vol. 82, no. 2, pp. 1287–1299, Apr. 2010.

[3] Y. Kwon, L. A. Vazquez-Zuniga, K. Park, S. Lee, H. Chang, and Y. Jeong, "Combinatorial study of supercontinuum generation dynamics in photonic crystal fibers pumped by ultrafast fiber lasers," *IEEE J. Quantum Electron.*, vol. 52, no. 6, pp. 1–11, Jun. 2016.

[4] J. K. Ranka, R. S. Windeler, and A. J. Stentz, "Visible continuum generation in air–silica microstructure optical fibers with anomalous dispersion at 800 nm," *Opt. Lett.*, vol. 25, no. 1, pp. 25–27, Jan. 2000.

[5] K. Shi, P. Li, S. Yin, and Z. Liu, "Chromatic confocal microscopy using supercontinuum light," *Opt. Express*, vol. 12, no. 10, pp. 2096–2101, May 2004.

[6] C. F. Kaminski, R. S. Watt, A. D. Elder, J. H. Frank, and J. Hult, "Supercontinuum radiation for applications in chemical sensing and microscopy," *Appl. Phys. B, Lasers Opt.*, vol. 92, no. 3, pp. 367–378, Sep. 2008.

[7] N. M. Israelsen *et al.*, "Real-time high-resolution mid-infrared optical coherence tomography," *Light Sci. Appl.*, vol. 8, no. 1, p. 11, 2019.

[8] A. Labruyère, A. Tonello, V. Couderc, G. Huss, and P. Leproux, "Compact supercontinuum sources and their biomedical applications," *Opt. Fiber Technol.*, vol. 18, no. 5, pp. 375–378, Sep. 2012.

[9] Y. Kwon, K. Park, S. Hong, and Y. Jeong, "Numerical study on the supercontinuum generation in an active highly nonlinear photonic crystal fiber with flattened all-normal dispersion," *IEEE J. Quantum Electron.*, vol. 53, no. 5, Oct. 2017, Art. no. 6100308.

[10] Y. Kwon, L. A. Vazquez-Zuniga, S. Lee, H. Kim, and Y. Jeong, "Numerical study on multi-pulse dynamics and shot-to-shot coherence property in quasi-mode-locked regimes of a highly-pumped anomalous dispersion fiber ring cavity," *Opt. Express*, vol. 25, no. 4, pp. 4456–4469, Feb. 2017.

[11] L. A. Vazquez-Zuniga *et al.*, "W-type highly erbium-doped active soft-glass fibre with high nonlinearity," *Electron. Lett.*, vol. 52, no. 12, pp. 1047–1048, Jun. 2016.

[12] C. Lei, A. Jin, R. Song, Z. Chen, and J. Hou, "Theoretical and experimental research of supercontinuum generation in an ytterbium-doped fiber amplifier," *Opt. Express*, vol. 24, no. 9, pp. 9237–9250, May 2016.

[13] C. Lei, R. Song, Z. Chen, D. Pu, and J. Hou, "Supercontinuum generation in an ytterbium-doped fiber amplifier with cascaded double-clad passive fiber tapers," *IEEE Photon. J.*, vol. 9, no. 2, Apr. 2017, Art. no. 1501409.

[14] C. Louot *et al.*, "Supercontinuum generation in an ytterbium-doped photonic crystal fiber for CARS spectroscopy," *IEEE Photon. Technol. Lett.*, vol. 28, no. 19, pp. 2011–2014, Oct. 1, 2016.

[15] T. Schreiber, J. Limpert, H. Zellmer, A. Tünnermann, and K. P. Hansen, "High average power supercontinuum generation in photonic crystal fibers," *Opt. Commun.*, vol. 228, nos. 1–3, pp. 71–78, Dec. 2003.

[16] M. Tao *et al.*, "Super-flat supercontinuum generation from a Tm-doped fiber amplifier," *Sci. Rep.*, vol. 6, no. 1, Apr. 2016, Art. no. 23759.

[17] A. M. Heidt, "Pulse preserving flat-top supercontinuum generation in all-normal dispersion photonic crystal fibers," *J. Opt. Soc. Amer. B, Opt. Phys.*, vol. 27, no. 3, pp. 550–559, Mar. 2010.

[18] F. R. Arteaga-Sierra, A. Antikainen, and G. P. Agrawal, "Dynamics of soliton cascades in fiber amplifiers," *Opt. Lett.*, vol. 41, no. 22, pp. 5198–5201, Nov. 2016.

[19] Z. Huang *et al.*, "Combined numerical model of laser rate equation and Ginzburg–Landau equation for ytterbium-doped fiber amplifier," *J. Opt. Soc. Amer. B, Opt. Phys.*, vol. 29, no. 6, pp. 1418–1423, Jun. 2012.

[20] K. Park, H. Kim, M. Yeo, and Y. Jeong, "Quantum-coherent supercontinuum generation in active highly nonlinear photonic crystal fibers," in *Proc. 10th Int. Conf. Adv. Infocomm Technol. (ICAIT)*, Aug. 2018, pp. 204–208.

[21] G. Agrawal, *Applications of Nonlinear Fiber Optics*. Amsterdam, The Netherlands: Elsevier, 2001.

[22] J. T. Manassah and B. Gross, "Propagation of femtosecond pulses in a fiber amplifier," *Opt. Commun.*, vol. 122, nos. 1–3, pp. 71–82, Dec. 1995.

[23] S. Chi, C.-W. Chang, and S. Wen, "Femtosecond soliton propagation in erbium-doped fiber amplifiers: The equivalence of two different models," *Opt. Commun.*, vol. 106, nos. 4–6, pp. 193–196, Mar. 1994.

[24] G. P. Agrawal, *Nonlinear Fiber Optics*, 4th ed. San Francisco, CA, USA: Academic, 2007.

[25] G. J. D. Valcárcel, E. Roldán, and F. Prati, "Semiclassical theory of amplification and lasing," *Revista mexicana de física E*, vol. 52, no. 2, pp. 198–214, 2006.

[26] M. Horowitz, C. R. Menyuk, and S. Keren, "Modeling the saturation induced by broad-band pulses amplified in an erbium-doped fiber amplifier," *IEEE Photon. Technol. Lett.*, vol. 11, no. 10, pp. 1235–1237, Oct. 1999.

[27] L. W. Liou and G. P. Agrawal, "Solitons in fiber amplifiers beyond the parabolic-gain and rate-equation approximations," *Opt. Commun.*, vol. 124, nos. 5–6, pp. 500–504, Mar. 1996.

[28] R. Poozesh, K. Madanipour, and P. Parvin, "High SNR watt-level single frequency Yb-doped fiber laser based on a saturable absorber filter in a cladding-pumped ring cavity," *J. Lightw. Technol.*, vol. 36, no. 20, pp. 4880–4886, Oct. 15, 2018.

[29] J. Hult, "A fourth-order Runge–Kutta in the interaction picture method for simulating supercontinuum generation in optical fibers," *J. Lightw. Technol.*, vol. 25, no. 12, pp. 3770–3775, Dec. 2007.

[30] A. V. Gorbach and D. V. Skryabin, "Light trapping in gravity-like potentials and expansion of supercontinuum spectra in photonic-crystal fibres," *Nature Photon.*, vol. 1, no. 11, pp. 653–657, Nov. 2007.

[31] R. Driben, B. A. Malomed, A. V. Yulin, and D. V. Skryabin, "Newton's cradles in optics: From *N*-soliton fission to soliton chains," *Phys. Rev. A, Gen. Phys.*, vol. 87, no. 6, Jun. 2013.

[32] R. Driben, A. V. Yulin, A. Efimov, and B. A. Malomed, "Trapping of light in solitonic cavities and its role in the supercontinuum generation," *Opt. Express*, vol. 21, no. 16, pp. 19091–19096, Aug. 2013.

[33] D. R. Solli, C. Ropers, P. Koonath, and B. Jalali, "Optical rogue waves," *Nature*, vol. 450, no. 7172, p. 1054, 2007.

[34] R. Driben and I. Babushkin, "Accelerated rogue waves generated by soliton fusion at the advanced stage of supercontinuum formation in photonic-crystal fibers," *Opt. Lett.*, vol. 37, no. 24, pp. 5157–5159, Dec. 2012.

[35] S. Lee, K. Park, H. Kim, L. A. Vazquez-Zuniga, J. Kim, and Y. Jeong, "Intermittent burst of a super rogue wave in the breathing multi-soliton regime of an anomalous fiber ring cavity," *Opt. Express*, vol. 26, no. 9, pp. 11447–11457, Apr. 2018.

[36] T. G. Philbin, C. Kuklewicz, S. Robertson, S. Hill, F. Konig, and U. Leonhardt, "Fiber-optical analog of the event horizon," *Science*, vol. 319, no. 5868, pp. 1367–1370, Mar. 2008.

[37] S. Kivistö, R. Herda, and O. G. Okhotnikov, "All-fiber supercontinuum source based on a mode-locked ytterbium laser with dispersion compensation by linearly chirped Bragg grating," *Opt. Express*, vol. 16, no. 1, pp. 265–270, 2008.

[38] J. Price, W. Belardi, T. Monro, A. Malinowski, A. Piper, and D. Richardson, "Soliton transmission and supercontinuum generation in holey fiber, using a diode pumped Ytterbium fiber source," *Opt. Express*, vol. 10, no. 8, pp. 382–387, Apr. 2002.

[39] C.-H. Yeh, C.-C. Lee, and S. Chi, "120-nm bandwidth erbium-doped fiber amplifier in parallel configuration," *IEEE Photon. Technol. Lett.*, vol. 16, no. 7, pp. 1637–1639, Jul. 2004.

[40] Y. Kodama and A. Hasegawa, "Nonlinear pulse propagation in a monomode dielectric guide," *IEEE J. Quantum Electron.*, vol. QE-23, no. 5, pp. 510–524, May 1987.